Air-gap Magnetic Field Design Optimization for U-shaped Ironless Permanent Magnet Linear Synchronous Motors

Peng Sun, Huixing Zhou
Department of Mechanical Design and Manufacturing, China Agricultural University, Beijing, 100083, China

***Abstract*-A U-shaped ironless permanent magnet linear synchronous motor, made by our group, is studied in this paper. The magnetic flux density stabilization is a primary problem, as the air-gap magnetic field with normal component of flux density of longitudinal sine and latitudinal uniformity is required for many precise positioning systems. We proposed a design optimization to improve the magnetic flux density and reduce magnet volume by defining a flexible objective function, where a genetic algorithm was used to find the optimal motor dimensions. The design optimization was verified by a layered finite element analysis, which could lower the complexity of the magnetic field analysis. And experimental results of the prototype were provided to illustrate the effectiveness of the proposed idea.**

Nomenclature and Abbreviations

x	longitudinal coordinate
y	transverse coordinate
z	normal coordinate
B_x	longitudinal component of the air-gap magnetic flux density
B_z	normal component of the air-gap magnetic flux density
A	magnetic vector potential
F_r	thrust ripple function
PM	permanent magnet
V_M	volume of PM
h_M	height of PM
w_M	width of PM
l_M	length of PM
g	air-gap length
τ	pole pitch
m	No. of phases
q	No. of coils per pole per phase
B_r	remanence of the PM
H_{cj}	coercive force of the PM
η	magnet width to pole pitch ratio
M	multi-objective function
PMLSM	permanent magnet linear synchronous motor
UIPMLSM	U-shaped ironless PMLSM
LFEA	layered finite element analysis
3DFEA	three-dimensional finite element analysis

I. INTRODUCTION

Permanent magnet linear synchronous motors (PMLSMs) are probably the most naturally applicable to applications involving high speed and high precision motion control, such as semiconductor processes, electronics board assembly, precision metrology and micro & nano motion control. As PMLSMs enjoy the main benefits include high force density, high dynamic performance, low thermal losses, and most importantly, the high precision and accuracy associated with the simplicity in mechanical structure. Traditionally, the iron-core PMLSM gained more attraction because of the high developed motor thrust. However the thrust ripple is a major weakness of the iron-core PMLSM for precise positioning systems like what mentioned above. As the internal factors were considered, there are three main factors that result in the force ripple. They are respectively the detent force due to slotted topologies and finite length of moving part, asymmetric phase windings, and the rather large attracting force which is a normal force to induce additional friction force and is not desirable for motor motion. Recently, the U-shaped ironless PMLSM (UIPMLSM) has been rapidly developed.

Generally speaking, the UIPMLSM inherits the benefits of PMLSM. And compared to the iron-core PMLSM, the UIPMLSM has predominant advantages such as the lack of the detent force, no attracting force as well as negligible iron loss, because the UIPMLSM have symmetrical topologies of magnets and the lack of primary iron core and teeth. However, there are still several factors which result in undesirable performance and high production cost, such as higher harmonics, relatively low thrust ripple due to distortion of sinusoidal distribution of the air-gap magnetic flux density, larger non-ferromagnetic air gap which requires more PM material for higher thrust density. Therefore, high thrust density, low thrust ripple, and economical magnet consumption are required to be paid more attention when designing UIPMLSMs. Unfortunately, there exists no general condition to meet all the expected at the same time. An improvement of each objective may be a reduction to the others. A balance among these objectives is required. Hence, a multi-objective design optimization is proposed.

In this paper, we take the magnetic flux density stabilization as a primary problem. At first, a layer model was used in

defining the optimization problem [1], [2]. Then, a multi-objective function was defined to increase the amplitude of the air-gap magnetic flux density and reduce the force variations and magnet volume with appropriate constraints. The PM dimensions and air-gap length are chosen as design variables. This optimization reduced magnetic flux density pulsations and magnet volume, while keeping relatively high amplitude for the sinusoidal distribution of the air-gap magnetic flux density. A genetic algorithm was employed to search for the optimal design values. The layered finite element analysis (LFEA) was introduced to reduce the complexity and time-consumption of three-dimensional finite element analysis (3DFEA). Finally, a motor prototype with optimal dimensions was made for experiments to verify the air-gap magnetic field design optimization.

II. Analytical Model of UIPMLSM

A. The Structure of the UIPMLSM

A schematic diagram of an UIPMLSM studied in this paper is presented in Fig. 1 (a). It consists of the external field excitation system and the internal three-phase armature. The U-shaped field excitation system is composed of back irons which looks like a capital letter U, and face-to-face surface-type PMs. The back iron is ferromagnetic and PMs are magnetized in the normal direction and located on the surface of the U-shaped yoke facing the armature. The PMs are equably arranged in one row, with symmetrical topologies and the stagger magnetic poles N, S,… N, S, as shown in Fig. 1 (b). The three-phase armature is made as coreless winding layer in which the input current waveforms are sinusoidal and produce a traveling magnetic field. Similar as the permanent magnet rotary synchronous motors, the thrust (named torque in rotary motors) is generated by the interaction between the permanent magnetic field and the traveling magnetic field, while the synchronous speed of the motor is the same as the speed of the traveling magnetic field [3].

The direction along the motion of coreless armature is defined as longitudinal or *x* coordinate. The direction along the motor width is defined as transverse or *y* coordinate. And the direction perpendicular to the foregoing *x*-*y* plane is defined as normal or *z* coordinate. Here, the *x*, *y*, and *z* coordinates compose the Cartesian coordinate system, as shown in Fig. 1 (b).

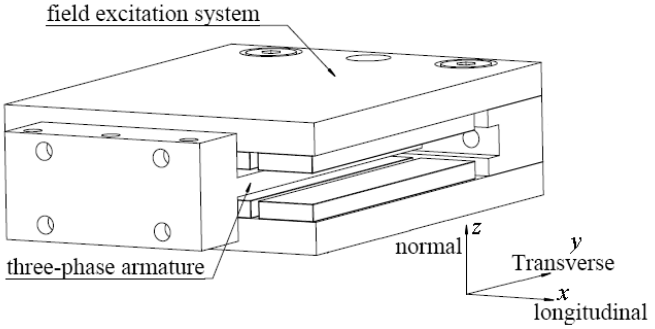

(a)

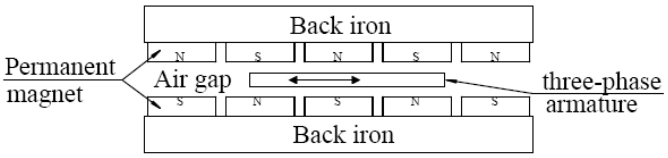

(b)

Fig. 1. Schematic diagram of the UIPMLSM.

B. Layer Model of the UIPMLSM

Fig. 2 shows a layer model of the UIPMLSM. In this model, we assume that motor length and permeability of the back iron are infinite. As the permeability of the not excited winding layer is the same as the air layer, we regard the winding layer and the air layer as an integrative air/winding layer, when analyzing the magnetic fields due to PMs. Thus only two regions are considered for the magnetic field analysis in this analytical model. Layer I and II in Fig. 2 represent the air/winding region and the permanent magnet region respectively.

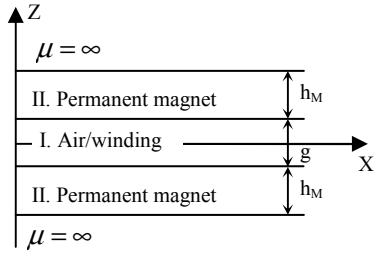

Fig. 2. Layer model of the UIPMLSM.

The problem can be simplified to a two-dimensional field distribution where the air-gap magnetic flux density has only two components, i.e., longitudinal component $\boldsymbol{B_x}$ and normal component $\boldsymbol{B_z}$. In this analysis, we assume that the magnetic flux density in the middle of air gap is sinusoidal with some higher harmonics and the magnetic saturation is neglected. Therefore, the $\boldsymbol{B_z}$ can be obtained as [4]

$$B_z = -\partial A / \partial x = -\sum_{n=1,3,\ldots}^{\infty} \frac{2n\pi}{\tau} C e^{-n\pi g/2\tau} \cos\left(\frac{n\pi x}{\tau}\right) \tag{1}$$

where $\boldsymbol{A}$ is magnetic vector potential in the air/winding layer, τ is pole pitch. The constant C is given by [1]

$$C = \frac{\frac{4B_r\tau}{n^2\pi^2}\sin(n\eta\pi/2)}{(e^{-n\pi g/\tau}+1)+\frac{\mu_M(e^{-n\pi g/\tau}-1)(e^{-2n\pi h_M/\tau}+1)}{\mu_0(e^{-2n\pi h_M/\tau}-1)}} \tag{2}$$

where η is magnet width to pole pitch ratio.

III. Magnetic Field Design Optimization with Multi-objective Function

A. Analysis of the UIPMLSM

In this paper, we take the air-gap magnetic flux density stabilization as a primary problem. The reasons are as follows. The motor developed thrust is directly proportional to the

normal component of the air-gap magnetic flux density. The thrust ripples can be reduced by the reduction of some higher flux harmonics. Proper PM dimensions can decrease magnet consumption. Hence, in other words, the design objectives are aim to increase the amplitude and reduce some higher flux harmonics for the sinusoidal distribution of the air-gap magnetic field flux density by choosing proper PM and air gap dimensions. Therefore, we need to identify the functional relations between the objectives and the air-gap magnetic flux density.

First of all, the $\boldsymbol{B_z}$ was described in (1). Then, the function $\boldsymbol{F_r}$ is employed as an indirect measure of the trust ripple as [1]

$$F_r = \frac{\sqrt{\sum_{n=5,7,11}^{\infty} B_{ng}^2}}{B_{1g}} \tag{3}$$

where $\boldsymbol{B_{ng}}$ is the $\boldsymbol{n}$th harmonics of the air-gap magnetic flux density. The multiples of the third harmonics components do not influence the machine operation because the motor includes a three-phase winding. Therefore, the value of $\boldsymbol{n}$ begins form 5 and omits three and multiples of three.

For surface magnets, the volume of PM $\boldsymbol{V_M}$ is as follows

$$V_M = p \times 2h_M \times w_M \times l_M \tag{4}$$

where $\boldsymbol{p}$ is the number of pole pairs. The $\boldsymbol{h_M}$, $\boldsymbol{w_M}$ and $\boldsymbol{l_M}$ stand for the height, width and length of PM respectively.

As stated previously, the multi-objective function $\boldsymbol{M}$ is thus proposed as follows

$$M = B_z^i \Big/ F_r^j V_M^k \tag{5}$$

where $\boldsymbol{B_z}$, $\boldsymbol{F_r}$ and $\boldsymbol{V_M}$ stand for the flux density, the thrust ripple function and the PM volume, respectively. The importance factors i, j, and k are chosen to determine the relative importance of thrust, thrust ripple and magnetic consumption in the multi-objective optimization [5].

Some principal values have been fixed for each motor design, which are listed in Table I. Some constraints should be taken into account during the optimization to prevent the possibility of reaching unrealistic optimization results. The limiting values of design variables are listed in Table II.

TABLE I
PRINCIPAL DATA OF THE UIPMLSM

Parameter	Value
Pole pitch	τ = 32 mm
Number of phases	m = 3
Number of coils per pole per phase	q = 1
Remanence of the PM	B_r = 1.4 T
coercive force of the PM	H_{cj} = 1350 KA/m

TABLE II
DESIGN VARIABLES CONSTRAINTS

Parameter	Symbol	Min	Max	Unit
Length of PM	l_M	65	100	mm
Width of PM	w_M	6	16	mm
Height of PM	h_M	2	6	mm
Air gap length	g	5	10	mm

The multi-objective function defined in (5) is particularly effective as its maximization fulfills all objectives of the optimization simultaneously, i.e., an increase in $\boldsymbol{B_z}$ and a reduction in $\boldsymbol{F_r}$ and $\boldsymbol{V_M}$. A genetic algorithm is used to find the optimal motor dimensions.

B. Genetic Algorithm

The genetic algorithm is a method for solving both constrained and unconstrained optimization problems which is based on natural selection [6]. The genetic algorithm repeatedly modifies a population of individual solutions. At each step, the genetic algorithm selects individuals at random from the current population to be parents and uses them to produce the children for the next generation. Over successive generations, the population evolves toward an optimal solution.

Here, we solve the problem with the assistance of the Multiobjective Genetic Algorithm Solver of Genetic Algorithm and Direct Search Toolbox™, MATLAB R2008a.

C. Multi-objective Optimization

Generally speaking, the values of i, j, and k depend on the requirement of the specific application and the designer's objectives. Here, the value of i = 1 is chosen to simplify the design. And more emphasis is placed on the magnetic consumption rather than the thrust ripple by choosing k=1.2 and j=0.6 [1], [5].

The results of the design optimization are listed in the fourth column of Table III. It can be seen that the multi-objective optimization increase flux density by 19.5% and reduces the thrust ripple and magnetic volume by 48.3% and 22.8% respectively compared to the specifications of the original motor.

TABLE III
DIMENSIONS OF MOTORS FOR MULTI-OBJECTIVE FUNCTION

Variables	Symbol	Original motor	Optimization	unit
Magnet length	l_M	85	75	mm
Magnet width	w_M	12	14	mm
Magnet height	h_M	6	4.5	mm
Airgap length	g	8	7	mm
Flux density	B_z	0.605	0.723	T
Thrust ripple	F_r	4.64	2.4	N
PM volume	V_M	85680	66150	mm^3

IV. DESIGN EVALUATION BY LFEA

As one of the numerical methods in magnetic field analysis, the finite element method is known as an accurate analysis method that can consider geometric details and the nonlinearity of magnetic material [7]. However, 2DFEA is relatively approximative and the more accurate 3DFEA is complex and requires long computation time especially at the initial design stage. Therefore, a LFEA is developed to avoid these shortcomings and employed to verify the design optimization in this section.

A. LFEA Concept

The LFEA is the improvement of 3DFEA. The LFEA consists of four basic steps, i.e., 3DFEA, defining layers and paths, data extraction and data processing. Firstly, the modeling, meshing and solution of 3DFEA of the motor are carried out without post-processing. Then, the solved motor model is divided into layers transversally. The structure of each layer is considered to

be steady transversally when the number of layers is lager enough. A series of intersecting lines between the two vertical planes, the layers and the *x-y* working plane in the middle of air gap, are defined as paths. Thirdly, the data, including the $\boldsymbol{B}_z$ and the longitudinal position along the defined paths, are extracted and exported to files in ASCII formats. Finally, the data from all layers are integrated into the whole graphical result which displays the 3D distribution of the normal component of magnetic flux density at the defined *x-y* working plane. The precision of LFEA depends on the number of layers and the number of samplings on the defined path.

B. LFEA Results

The motor was modeled with the optimized motor dimensions. The dimensions (length, width and height) of air hood should be three times as or more than those of the motor for the 3DFEA modeling. Since under the circumstances, the peripheral of air hood can be considered as the isosurface of magnetic potential to simplify the 3D open domain magnetic field problems [8]. Fig. 3 shows the schematic diagram for 3DFEA, including the whole model, the layers, the defined *x-y* working plane and paths.

The 3D distribution of the $\boldsymbol{B}_z$ at the defined *x-y* working plane, obtained by LFEA, is shown in Fig. 4. In Fig. 4a, there is some distortion of sinusoidal flux density distribution at the end due to the end effect and complex magnetic circuit relations. It can be seen in Fig. 4b that the $\boldsymbol{B}_z$ is longitudinally sinusoidal and transversely uniform at the main working region (x=0-35, y=10-65), which is required for many precise positioning systems.

C. Comparison with LFEA

As mentioned above, we take the magnetic flux density stabilization as the primary problem. Hence, the distributions of $\boldsymbol{B}_z$ obtained by analytical model and LFEA are compared for design evaluation.

Fig. 5 shows the distributions of $\boldsymbol{B}_z$ obtained by analytical model and LFEA along the defined path. It can be seen that the distributions of $\boldsymbol{B}_z$ obtained by analytical model and LFEA are in good agreement, and have a sinusoidal waveform with a 32mm period, which is corresponding to the magnetic pitch. The specific peak value of $\boldsymbol{B}_z$ obtained by LFEA is 0.784 T, and the error is less than 8% compared with that obtained by optimization design, as shown in Table IV. The result confirms the validity of the design optimization.

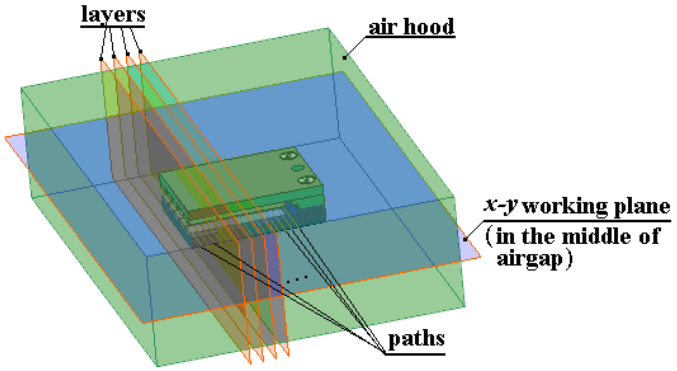

Fig. 3. Schematic diagram for 3DFEA.

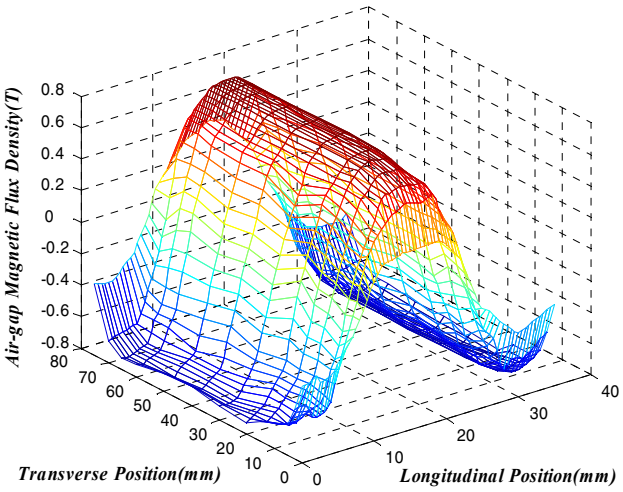

(a)

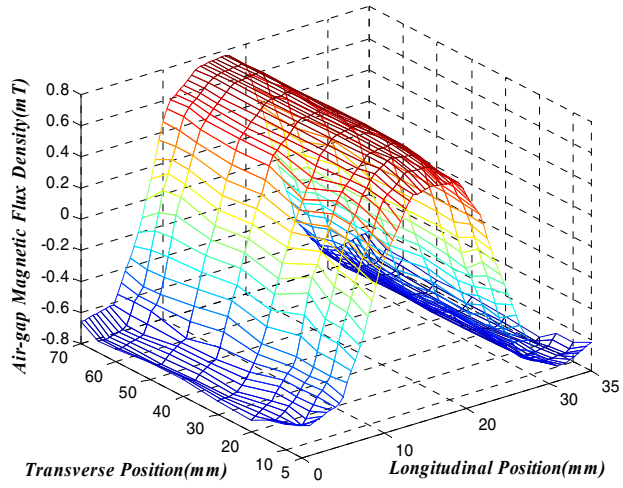

(b)

Fig. 4. 3D air-gap magnetic flux density distribution at the *x-y* working plane: (a) x=0-35, y=0-75, (b) x=0-35, y=10-65.

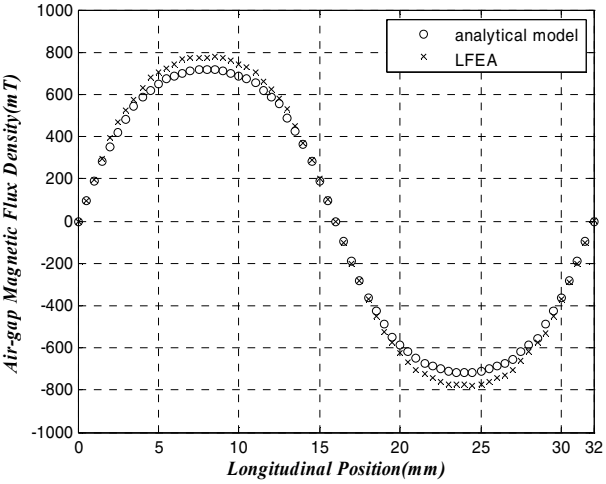

Fig. 5. The distribution of $\boldsymbol{B}_z$ along the defined path.

TABLE IV
COMPARISON OF OPTIMIZATION DESIGN, LFEA AND EXPERIMENTAL RESULTS

Results	Optimization design	LFEA	Experiment
Peak value of $\boldsymbol{B}_z$ (T)	0.723	0.784	0.7518

V. EXPERIMENT RESULTS AND DISCUSSION

A. Experiment Results

Finally, a motor prototype was manufactured with the optimized motor dimensions by our group. Fig. 6 is the photograph of the UIPMLSM prototype.

Here, we still take the $\boldsymbol{B}_z$ as the primary parameter into consideration. The $\boldsymbol{B}_z$ was detected using a SG-4L type digital teslameter with 1μT resolution and 0.5% accuracy (Beijing Zhuoshengjia Magnetic Technology Co., Ltd., China), and the result is presented in Fig. 7. The peak value of the $\boldsymbol{B}_z$ distribution of motor prototype is 0.7518 T, as listed in the fourth column of Table IV. The result obviously means an increase in magnetic flux density by 24.3% compared to that of the original motor.

The Fourier transform was employed to find the amplitude spectrum of $\boldsymbol{B}_z$. Fig. 8 is the Fourier transform result for the $\boldsymbol{B}_z$ distribution of motor prototype. The main reason that the amplitudes are not exactly at the given point is because of the noise existing. And it can be easily seen that the ratio of higher harmonics to fundamental wave is less than 5%. Therefore, the motor with the optimized dimensions provides reduced flux density pulsations substantially.

B. Discussion

The result we have obtained suggests that the magnetic flux density stabilization has a significant effect on the motor performance as the internal factor, because the air-gap flux density contributes to the developed motor force directly. The improvement of magnetic flux density can improve the motor performance radically. On the other hand, there are some external factors in practical operation, such as payload variation, unknown nonlinearities and disturbances. Thus, the connection of motor optimization designs and control schemes will produce the desired results for more precise positioning systems.

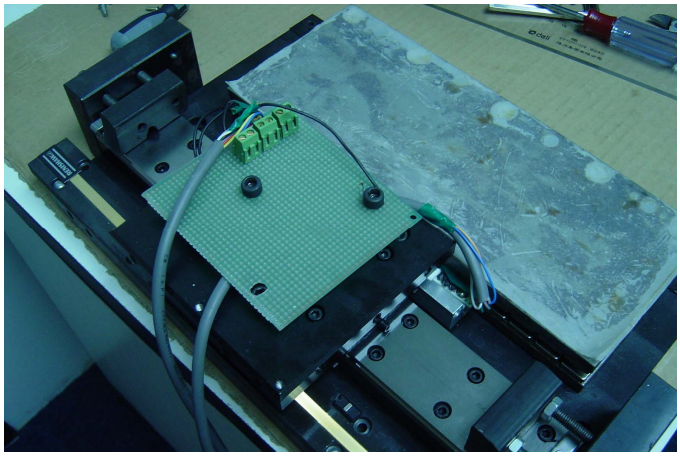

Fig. 6. UIPMLSM prototype

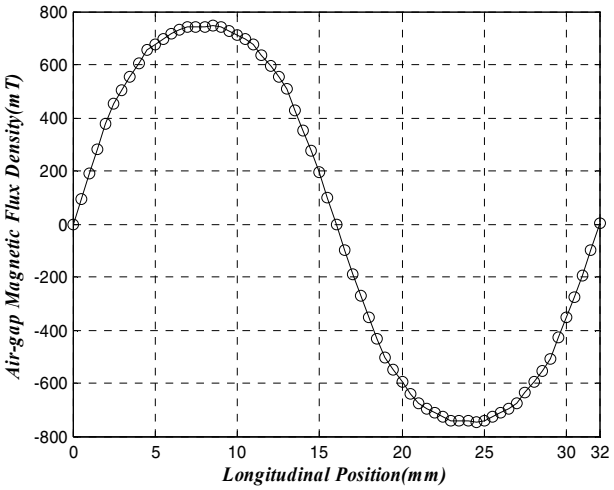

Fig. 7. The $\boldsymbol{B}_z$ distribution of the prototype.

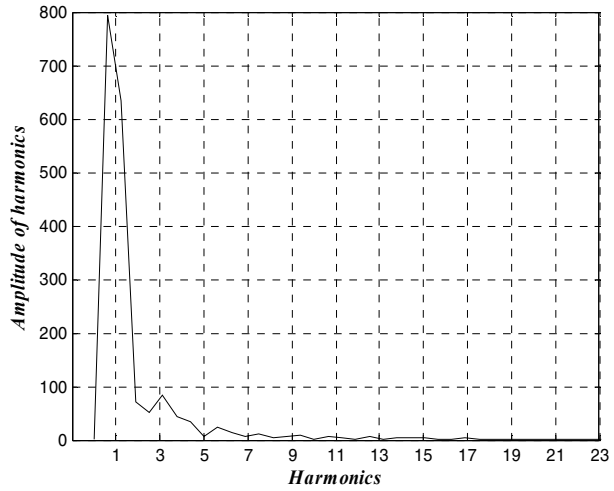

Fig. 8. Single-sided amplitude spectrum of $\boldsymbol{B}_z$.

VI. CONCLUSION

The design optimization of high thrust density, low thrust ripple, and economical magnet consumption based on the layer model for UIPMLSM is presented in this paper. A genetic algorithm is used to find the optimized PM dimensions. The LFEA is developed and employed to evaluate and confirm the validity of the design optimization. A motor prototype was manufactured with the optimized motor dimensions. Experimental results indicated that the multi-objective function can achieve all the expected of the air-gap magnetic field design optimization for UIPMLSM simultaneously.

ACKNOWLEDGMENT

Financial support was provided by WinnerMotor Direct Drive (Beijing) Technology Co., Ltd.

REFERENCES

[1] S. Vaez-Zadeh, and A. H. Isfahani, "Multiobjective design optimization of air-core linear permanent-magnet synchronous motors for improved thrust and low magnet consumption," *IEEE Trans. Magn.,* vol. 42, no. 3, pp.

446-452, March 2006.
[2] S. M. Jang, et al., "Analysis of the tubular motor with Halbach and radial magnet array," in *Proceedings of the. ICEMS 2003*, Nov. 2003, pp. 250-252.
[3] J. F. Gieras, and Z. J. Piech, *Linear Synchronous Motors: Transportation and Automation Systems,* vol. 2. Florida: CRC, 2000, pp. 1-4.
[4] M. J. Chung, M.G. Lee, et al., "Analytical representation of cogging force in linear brushless permanent magnet motor," in *Proceedings of the. ICMT'99*, Oct. 1999, pp. 310-314.
[5] S. Vaez-Zadeh and A. R. Ghasemi, "Design optimization of permanent magnet synchronous motors for high torque capability and low magnet volume," *Elect. Power Syst. Res.*, vol. 74, pp. 307–313, Mar. 2005.
[6] Shan Shi, Q. Li and X. wang, "Design Optimization of Brushless Direct Current Motor Based on Adaptive Genetic Algorithm," *Journal of Xi ′ an Jiaotong University,* vol. 36, No. 12, pp. 1215-1218, Dec. 2002 (in Chinese).
[7] Gyu-Hong Kang, Jung-Pyo Hong, and Gyu-Tak Kim, "A novel design of an air-core type permanent magnet linear brushless motor by space harmonics field analysis," *IEEE Trans. Magn.,* vol. 37, no. 5, pp. 3732-3736, September 2001.
[8] Xiaoyuan Wang, Renyuan Tang and etal., "Optimization of Disk Coreless Permanent Magnet Synchronous Motor Based on Halbach—the Wedgy Airgap Motor," *Transactions of China Electrotechnical Society.*, vol. 22, no. 3, pp. 2–5, Mar. 2007 (in Chinese).